International Journal of Thin Films Science and Technology

http://dx.doi.org/10.18576/ijtfst/140203

Mechanistic Study of Fluoride Removal from Aqueous Media Using Chemically Modified Chitosan@Zirconium Adsorbent

Sandip H. Bhatt[1,2] *and Kamlesh Gurjar*[3,*]

[1] Gujarat Technological University, Ahmedabad, Gujarat, 382424, India
[2] Chemical Engineering Department, L.D. College of Engineering, Ahmedabad, Gujarat, India
[3] Department of Science and Humanities, Vishwakarma Government Engineering College, Ahmedabad, Gujarat, 382424, India

Received: 8 Jun. 2024, Revised: 22 Sep. 2024, Accepted: 24 Jan. 2025
Published online: 1 May 2025

Abstract: In this investigation, we discussed the mechanistic analysis of the adsorption process employing chemically modified chitosan, conjugated with zirconium (Ch@Zr), for the removal of fluoride from aqueous solutions. The chitosan was chemically modified through microwave-assisted heating, while zirconium binding was accomplished using conventional chemical techniques to improve its fluoride adsorption efficacy. The adsorption mechanism was elucidated through a series of experimental procedures and analytical techniques, including surface characterization. Various parameters such as adsorbent dosage, pH, temperature, initial fluoride concentration, and contact time were systematically studied to optimize the adsorption process. The findings demonstrate that the modified Chitosan@zirconium exhibits a superior fluoride adsorption capacity, achieving maximum removal efficiency under optimized conditions. The adsorption process was evaluated using isotherm and kinetic models, including Freundlich and Langmuir isotherms, pseudo-second-order kinetics, Elovich model, and Weber's intraparticle diffusion model. This mechanistic insight contributes to the remediation of fluoride-contaminated wastewater by providing valuable information for developing effective fluoride removal strategies utilizing modified chitosan.

Keywords: Adsorption, Chitosan, zirconium, pseudo-second-order, Langmuir isotherms, Freundlich isotherms.

1 Introduction

Drinking water may contain fluoride; at nearly 0.7 mg L−1, it is considered beneficial and micronutrient however, if it exceeds 1.5 mg L−1, the World Health Organization (WHO) suggests that it be dangerous [1, 2]. One of the main sources of drinkable water, drinking groundwater, exposes people to excessive fluoride concentrations, which can lead to brain damage in severe cases of fluorosis, which causes abnormalities in the human teeth and bones. The condition fluorosis is irreversibly caused by the excess fluoride present in drinking water [3,4].

To remove excess fluoride from water, some conventional methods include the ion-exchange method, membrane separation, chemical precipitation, electrocoagulation, and adsorption [5-9]. Of them, adsorption is considered a promising and versatile method due to its ease of use, speed, affordability, and ease of handling. Most promising thing is the cost effectiveness of this method using biomaterial, waste, and other low-cost materials. Currently, numerous adsorbent materials have been applied for removal of fluoride from aqueous media, such as activated alumina, activated carbon, clay materials, polymer-doped adsorbents, and metal oxides [10-12]. Most of them are used as industrial adsorbents and they are not cost effective and selective. Each class of adsorbent have some limitations. Nevertheless, a few of these classes of materials are limited in many ways, including poor surface area, pore size, and low selectivity. Biopolymeric adsorbents are an attractive class of fluoride removal and other potential environmental pollution prevention applications [13-16]. Chitosan is one of the most widespread biopolymers on the globe, making it an attractive choice for water treatment in general [17]. Chitosan (CS) is an N-deacetylated derivative of the natural polysaccharide chitin and is rich in free amino acids. The-NH2 group in chitosan is more reactive, easy to be chemically modified, and exhibits high adsorption potential [18-20].

Chitosan biopolymer is a nontoxic, biocompatible, biodegradable, and antibacterial amino polysaccharide. Traditional chemical techniques and microwave synthesis can easily achieve physical and chemical alterations that eliminate the practical application limitations of chitosan. Chitosan based biopolymers are typical class of adsorbent are used to reduction fluoride concentration in water body and industrial waste water. To enhance these chitosan qualities, many fresh cross-linkers have been developed

*Corresponding author E-mail: gurjar.kamlesh@gmail.com

today, coupled with new crosslinked chitosan derivatives [21, 22].

On the other hand, Fluoride ions in water have a strong affinity with positively charged elements with great affinity towards electropositive and positive charge ions like ca^{+2} and Zr^{+4}. However, due to their significant affinity for fluoride ions especially, materials containing rare earth elements have been promising adsorbents [23, 25]. Regarding this, the fluoride removal properties of multivalent metals such Al (III), Y(III), La (III), Ce (IV), and Zr (IV) in the form of oxides, hydrous oxides, and basic carbonates are being examined. Zirconium is an exciting element that belongs to rare earths with a strong affinity for fluoride [26-29].

In general, zirconium is less toxic when used alone or in combination, and there is not much proof of it being harmful when swallowed. Previous study has evaluated the capacity of cashew nutshell carbon coated with zirconium to eliminate fluoride from aqueous solutions [30-33]. Gao et al. developed a zirconia/zeolite composite to capture fluoride from water [34]. Rahman et al. synthesized a novel composite by doping polypyrrole with zirconium (IV) and zirconium (IV) iodate, optimizing it for enhanced fluoride adsorption properties [35]. Zhang et al. fabricated a zirconium-chitosan membrane integrated with graphene oxide (GO) for effective fluoride removal [36]. Prathibha et al. developed a Zr (IV)-functionalized sand composite, incorporating graphene oxide (GO), to enhance the efficacy of fluoride removal [37].

This work delves into a higher regeneration capacity of up to 96.2% with sodium hydroxide in a time period of 3 hours. Lewis acid Zr (IV) has a higher oxidation/valance state and is a member of the d-block elements, which can be preferentially attached to electronegative atoms like fluorine. To overcome the limitation of chitosan's relatively poor strength in acidic pH and the fact that zirconium compounds have a tendency to leach in solution, both difficulties can be resolved with the chemical binding of zirconium with the free -NH_2 in the side chain of chitosan. The synthesis, characterization, and fluoride adsorption properties of a novel zirconium–ethylenediamine-Chitosan (Zr@Ch-EDA) hybrid sorbent is reported in this article. Fluoride removal experiments were performed in bath mode.

2. Materials and methods:

2.1 Materials

Deacetylated chitosan (CS), Zirconium tetrachloride and ethylene diamine were procured fromTCI chemicals. The details of the chemicals used are shown in Table S1 (Supporting Information)

2.2 Preparation of adsorbent.

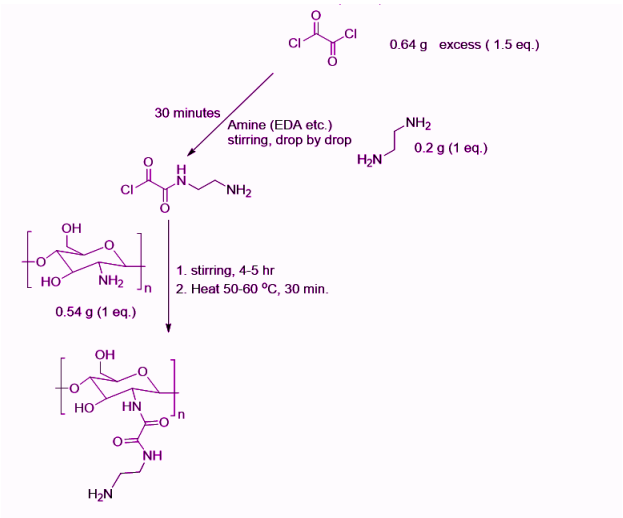

Fig. 1: Synthesis of EDA-Ch

2.3 Synthesis of EDA-Ch@Zr sorbent

As per Scheme 1, chemical modifications have been achieved, followed by the addition of zirconium tetrachloride in a small quantity in 30 minutes.in next step 20 minutes of sonication given to reaction mixture to improve homogeneous nature. A ratio of 1:1 is maintained with chemically modified chitosan and zirconium tetrachloride. 30 minutes of sonication provide the reaction mixture, followed by 2 hours (at room temperature) of continuous stirring at 700 rpm. Solid adsorbent recovered from reaction mixture solution, adjusting neutral to slightly basic (pH = 7 to 8).

2.4 Batch Studies for Fluoride Adsorption.

A fluoride ion stock solution (100 mg L−1) of NaF was prepared in deionized water, and the test solutions were made by subsequent dilution of the fluoride solution.

Samples of 0.1 to 0.5g of EDA-Ch@Zr were added to 100 mL of fluoride solution (5 to 50 mgL−1) to conical-bottom polypropylene tubes. The solution's pH was adjusted daily to 7.0 ± 0.25 using 0.1 N HCl or NaOH, and all the experiments were monitored until equilibrium was achieved.

The fluoride concentration was measured by 4500-F D. SPADNS Method (Ref. Std. Methods-23rd Edition). All measurements were carried out at 25 °C, and the adsorption capacity (qe, mg g−1) was calculated as follows

$$q_e = (C_0 - C_e) \times V/W$$

where V is the total solution volume, W is the mass of adsorbent, and C0 and Ce are the initial and final (or equilibrium) fluoride concentrations, respectively.

The experimental adsorption data was fitted by the Langmuir and Freundlich isotherm models expressed as

$$q_e = KC_e^n$$

$$q_e = \frac{q_{max} b C_e}{1 + bC_e}$$

where qmax is the maximum adsorption capacity (mg g−1), and b (L mg−1) the Langmuir constant related to the adsorption energy or affinity. On the other hand, K (mg1−1/nL1/n g−1) and n are Freundlich constants related to the adsorption capacity and the adsorption intensity, respectively.

3. Results and discussion:

3.1 FTIR Analysis

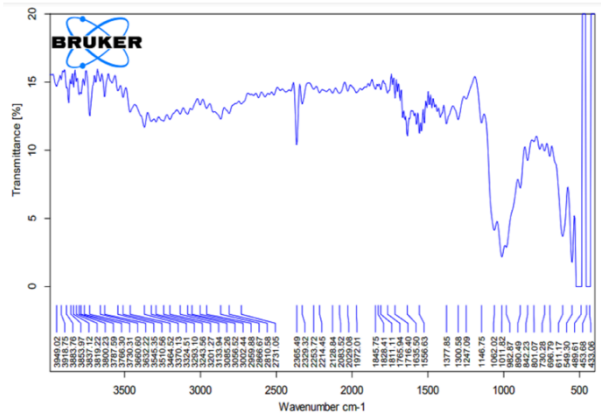

(a)

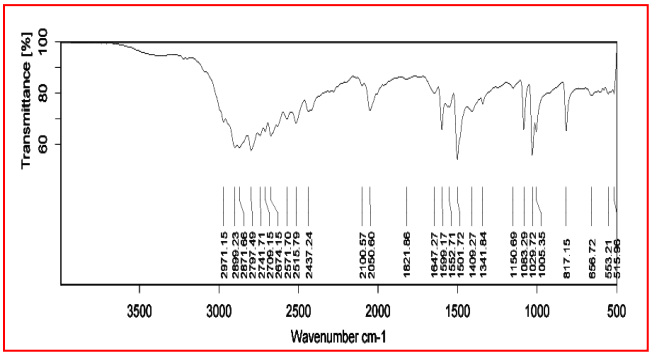

(b)

Fig. 2: (a) Chitosan (b) Ch-EDA FTIR spectrum

With FTIR data, differentiate EDA (Ethylene Diamine) modified chitosan from unmodified chitosan by identifying the following different peaks: The appearance of new peaks in the 1550–1650 cm–1 range, which are ascribed to the amide bond between EDA and chitosan's C=O stretching vibration. Greater peak intensity at 1647 cm^{-1} (amide I bond C=O stretching) in contrast to unmodified chitosan. A peak that could arise between 2800 and 2900 cm-1 and correspond to the EDA molecule's C-H stretching vibration.

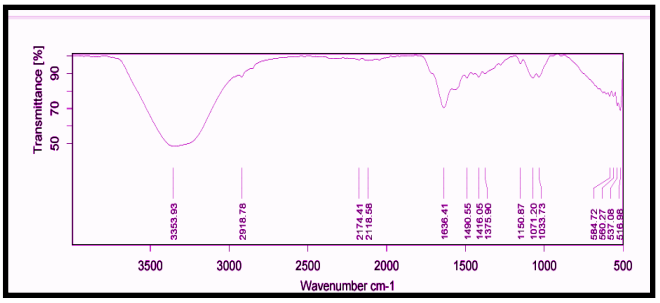

Fig. 3: EDA-Ch@Zr

FTIR spectrum data changed when EDA-Ch reacted with zirconium chloride. In the fingerprint region, a number of peaks were observed in unmodified chitosan, while in EDA-modified chitosan, a less intense peak is shown in this region. On the next modification with zirconium, the FTIR spectra, as per Figure 2, become more intense with additional peaks. It shows zirconium may react with an amine group due to this at the 580–620 cm^{-1}, Zr–N stretching vibration, indicating the formation of a zirconium-nitrogen bond with the modified side chain of the chitosan molecule. Also, the peaks become more intense in the range of 514 to 580 cm^{-1}.

3.2 Fluoride Analysis

The Fluoride Concentration determined by SPADNS method as per 4500-F D std. methods -23rd Edition and for higher concentration dilution method adopted calibration curve prepared with standard fluoride solution with 0 to 1.4 PPM as per Figure-3 Calibration curve plotted using statistical tool Origin pro-2024.

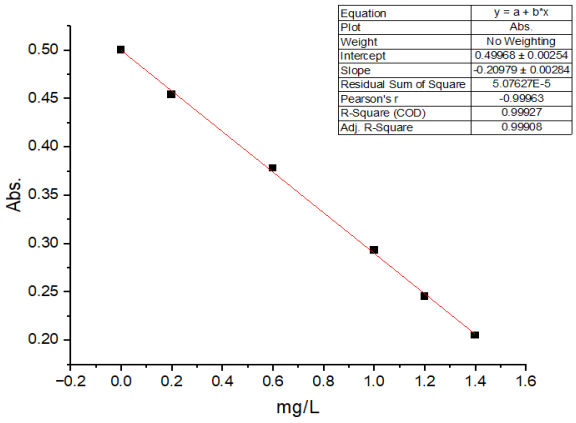

Fig. 4: Calibration curve

3.3 Adsorption kinetics and isotherm studies of fluoride removal

3.3.1 Linear and nonlinear PFO and PSO model

The effects of contact time, adsorbent dosage, pH, and starting concentration range were thoroughly investigated in the current publication. In order to improve understanding of the adsorption behaviour and fluoride removal of synthesised material (EDA-Ch@zr), the

isotherm model, pseudo-first-order (PFO), and pseudo-second-order (PSO) kinetic models were tested.

Using existing adsorption data, pseudo-first order and pseudo-second order models were used to determine the corresponding adsorption kinetics parameter. The pseudo-first-order and pseudo-second-order linear equations are shown in equation 1 and 2.

$$\ln (q_e - q_t) = \ln q_e - (k_1 t)/2.303 \quad (1)$$

$$t/q_t = 1/(k_2 q_e) + t/q_e \quad (2)$$

where q_e is he amount of fluoride adsorbed per unit weight of sorbent at equilibrium (mg / g), q_t is the amount of fluoride adsorbed per unit weight of sorbent at time t (min) and $k_1$and k_2 is the first and second order rate constant for the adsorption(min^{-1}) respectively.

In the batch kinetic investigation, varying dosages of EDA-CSA@Zr, ranging from 0.1 to 0.4 grams, were added to in a 4–30 PPM fluoride solution with 100 ml of volume, Ten millilitre samples were taken at various intervals (0–120 min) for fluoride measurement. The relationship between the fluoride adsorbed at the surface of EDA-Ch@Zr and its equilibrium concentration in the solution at constant temperature and pressure was described using adsorption isotherms.

The adsorption isotherm experiments were evaluated with an initial fluoride concentration range of 4 to 30 ppm. The adsorption of fluoride by EDA-Ch@Zr has been studied as a function of contact time with the aim to establish the adsorption kinetics and the adsorption equilibrium time. The relevant adsorption kinetics parameter was determined by employing the frequently employed pseudo-first-order and pseudo-second-order adsorption kinetic models. Pseudo-first-order model is followed by adsorption reaction preceded by diffusion through a boundary whereas pseudo-second-order model is commonly followed by adsorption process with chemisorption being the rate-control [29].

Khayyun *et.al* suggested that the adsorption model which best fits the experimental data has the ability to explain the adsorption better [38].

Y = -0.0479x + 0.472, R² = 0.9936

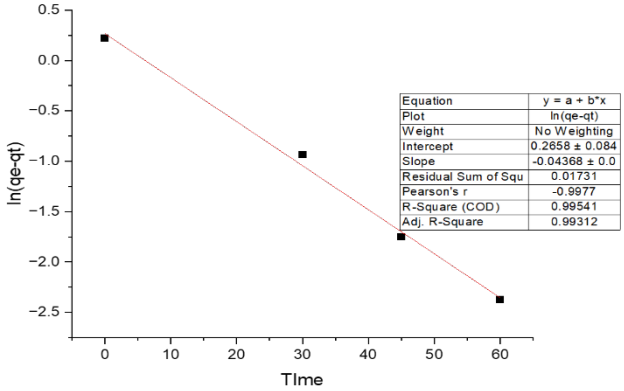

Linear pseudo-first-order kinetic model

Y = 0.86x+3.01, R² = 0.9636

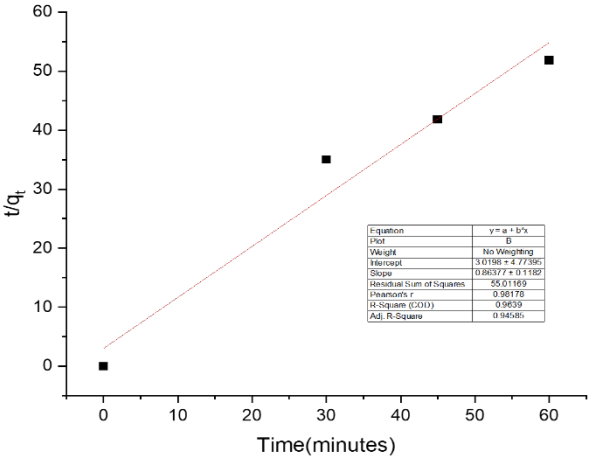

Linear Pseudo-second -order kinetic model

Fig. 5: Linear PFO & PSO model

Table 1: Linear PSO data

Linear PSO Data				
qe	Slope	Inrercept	h value	K
1.16	0.86	3.01	0.33	0.24

For PSO and PFO, both linear and nonlinear methods were applied in this study for calculating the adsorption kinetics parameter, which includes the correlation factor, qe, k, and h values.

The nonlinear pseudo-second-order model has a greater correlation coefficient (R2=0.99) than the pseudo-first-order model (R2=0.96), suggesting that it fits the fluoride adsorption better.

The PFO model has a negative slope value, which is not acceptable. Furthermore, the calculated adsorption amounts of the linear pseudo-second-order model (q_e, cal = 1.16 mg/g) agree well with the experimental values (q_e, expt = 1.15 mg/g) compared to the calculated adsorption amounts of the nonlinear pseudo-second-order model (q_e, cal = 1.79 mg/g), which were moderately higher than the value of the experimental adsorption capacity.

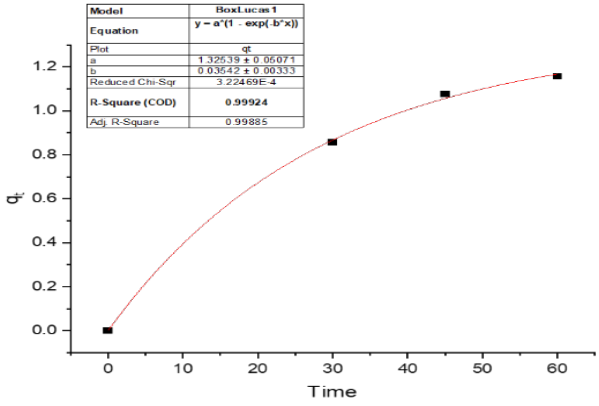

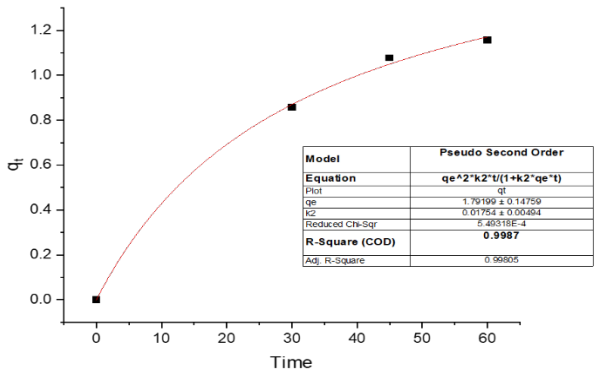

Fig. 6: Non-Linear PFO and PSO model

q_e = 1.79199 a = q_e = 1.33

K_2 = 0.01754 b= K_1 = 0.03542

The Nonlinear pseudo-second-order model predicts a higher equilibrium adsorption capacity and a slower approach to equilibrium compared to the pseudo-first-order model. This suggests that the adsorption process is likely dominated by chemisorption, which is more accurately described by the pseudo-second-order kinetics.

3.3.2 Weber–Morris- intraparticle diffusion kinetics model

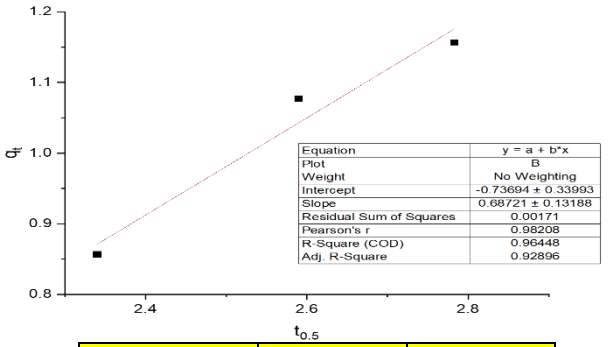

Slope	intercept	R^2
k=0.69	-0.74	0.9645

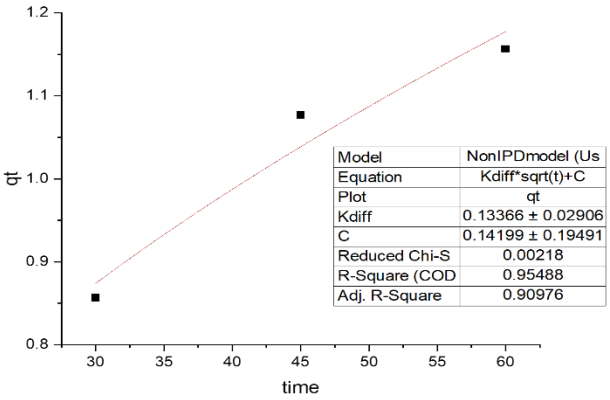

$K_{diif.}$	C	R^2
k=0.13	0.14	0.96

Fig. 7: Weber–Morris- intraparticle diffusion kinetics model

Weber-Morris established the intra-particle diffusion kinetic model, which explains the diffusion mechanism by which molecules of the adsorbate diffusion after adsorption on the surface, then diffuse into the adsorbent's pores.

$$q_t = k_{diff} . t^{0.5} + C$$

where C(mg/ g) is a constant that indicates the boundary layer thickness and may be found by plotting q versus t. where q(mg /g) is the amount of fluoride adsorbed at a time, and k(mg g hour) is the intraparticle diffusion rate constant. In accordance with this concept, the intra-particle diffusion process is not the rate-limiting step when a graph exhibits multi-linearity, indicating the involvement of different adsorption processes. The present studies revealed a multi-linear plot, indicating that the diffusion process happens over three steps. A distinct section that represents external mass transfer through instantaneous adsorption is shown in the first stage. The following step illustrates a slow adsorption process that serves as a rate-controlling step for intra-particle or pore diffusion. In the final stage, there is a plateau, or equilibrium stage, when diffusion slows down as the adsorbate content falls.

The fact that the linear IPD model graph wasn't passing through the origin indicates a complex process rather than intraparticle diffusion, which is the rate-limiting step.

3.4 Adsorption isotherm studies

The Three isotherm equations—Langmuir, Freundlich, and Temkin, were tested in the present research to evaluate different adsorption parameters through both linear and non-linear regression analysis.

Table 2: Adsorption isotherm parameters

	Freundlich Isotherm	Langmuir Isotherm	Temkin Isotherm
R^2	0.98335	0.84	0.9835
Slope	1.32293	4.4547	1.562
Intercept	0.7088	0.0589	-1.478
Constant	n = 0.76 k_f = 5.11	K_L= 3.81 R_{L1}= 0.14 R_{L2}= 0.062 R_{L3}= 0.003 R_{L4}= 0.49	BT(KJ/mol) = 1.562 KT_L (mg/L) = 0.4795

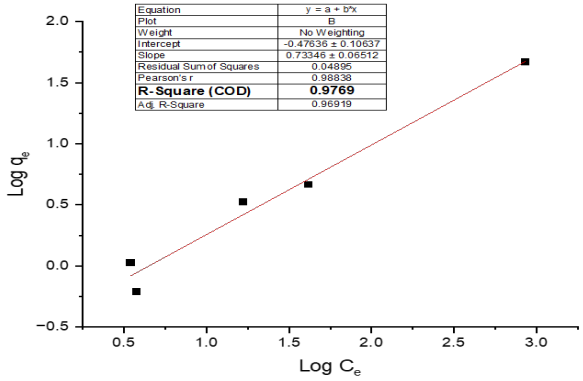

Fig. 8: Freundlich isotherm

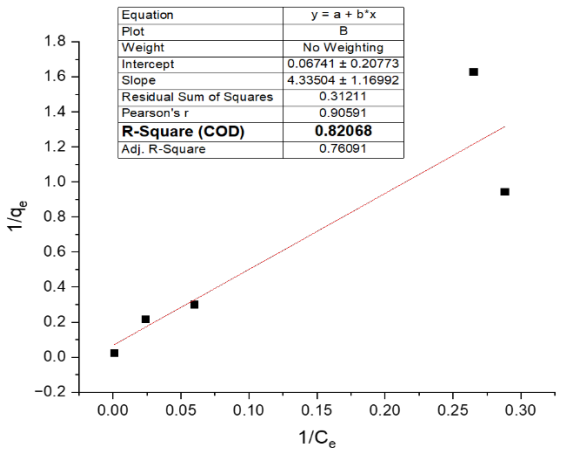

Fig. 9: Langmuir isotherm model

3.4.1 Langmuir isotherm model

One of the most commonly used models that postulates that adsorption results in the formation of a monolayer without interaction between the molecules of the adsorbate and all of the adsorption sites of the solid surface is the Langmuir model. This model relies on the concept that no strong bond may form on the adsorbate surface where all of the specific sites onto the adsorbent surface retain constant binding energy.

Table 2 contains a summary of the parameters that were determined based on the Adsorption fitting curves. Maximum adsorption capacity (q_{max}) and Langmuir constant (KL) were calculated from intercept and slope values. The values of Langmuir constants qm and (KL)relates to the capacity and energy of adsorption process. The isotherm criterion can be described by another dimensionless constant, which is

$$\mathbf{R_L = (1 + K_L/C_o)}$$

The R_L (dimensionless separation factor) values you provided for different initial concentrations under the Langmuir adsorption isotherm model indicate the favourability of adsorption at those concentrations R_L values less than 1 indicate favourable adsorption**.** R_L values slightly higher but still relatively low (0.49, 0.63) suggest moderate to favourable adsorption for initial concentrations of 7 ppm and 5 ppm, respectively. R_L values less than 1 (0.14, 0.06) indicate favourable adsorption for initial concentrations of 25 ppm, 60 ppm, respectively. The K_L value of 3.81 represents the adsorption capacity of the adsorbent. Higher KL values suggest higher adsorption capacity. The Q_{max} value of 16.97 mg/g represents the maximum amount of fluoride adsorbed per unit mass of adsorbent.

3.4.2 Freundlich isotherm.

The Freundlich isotherm model assumes that the adsorbate reaches to the non-uniform surface of the adsorbent with distinct adsorption sites having different adsorption energies. It assumes multilayer adsorption.

The linear equation for Freundlich isotherm model obtained to be y = 1.3293x + 0.7088. The gradient and y-intercept obtained from the graph were used to calculate relative adsorption capacity (KF) and intensity of adsorption (n).

Table 1 compares the Langmuir and Freundlich isotherm constants for the adsorption of fluoride onto Zr-EDA modified Chitosan (EDA-Ch@Zr).

The n value represents the heterogeneity of the surface sites and the degree of non-linearity in the adsorption process. n=1.36, value of n greater than 1 indicates favourable adsorption.

R2=0.9835, indicates that the linear fit explains 98% of the variability in Adsorption experiment data. The adsorption capacity (K) is relatively high, suggesting that your adsorbent has a good capacity for removing fluoride. The high $R2$ value indicates that the Freundlich model fits your data well, implying that the model adequately describes the adsorption behaviour of fluoride on to Zr-CSA adsorbent. Experimental data and calculated values suggest that the adsorption process for fluoride removal using this adsorbent follows Freundlich isotherm behaviour quite closely and has promising adsorption capacity.

3.4.3 Temkin isotherm

The Temkin isotherm assumptions are that the adsorption process is uniform, reversible. and continuous and adsorption energy decreases linearly with increasing surface coverage. The important parameters of the Temkin isotherm are:

B (Temkin constant): related to the adsorption energy and surface coverage

A (Temkin constant): related to the adsorption capacity.

The Temkin isotherm equation is:

$$q_e = (RT/B) \ln (A\ C_e)$$

where:

qe = adsorption capacity at equilibrium (mg/g)

Ce = equilibrium concentration of adsorbate (mg/L)

A = Temkin constant (L/mg)

B = Temkin constant (J/mol)

R = gas constant (8.314 J/mol·K)

T = temperature (K)

The Temkin isotherm graph plot is typically a curved line that represents the relationship between the adsorption capacity (qe) and the equilibrium concentration (Ce). The plot can be linearized by transforming the data into a linear form using the Temkin isotherm equation.

The linearized Temkin isotherm equation is:

$\ln(qe) = \ln(A) + (RT/B) \ln (Ce)$

Table 3: Temkin isotherm parameters

intercept	slope	BT (KJ/mol)	$KT_{L(}$ mg/L)	R^2
-1.1478	1.562	1.562	0.479588	0.9835

The BT value of **1.562** is obtained from the Temkin isotherm model. It represents the heat of adsorption (in kJ/mol) and provides insight into the energetics of the adsorption process. Higher BT values indicate stronger interactions between the adsorbate (fluoride) and the adsorbent zirconium-modified chitosan derivative.

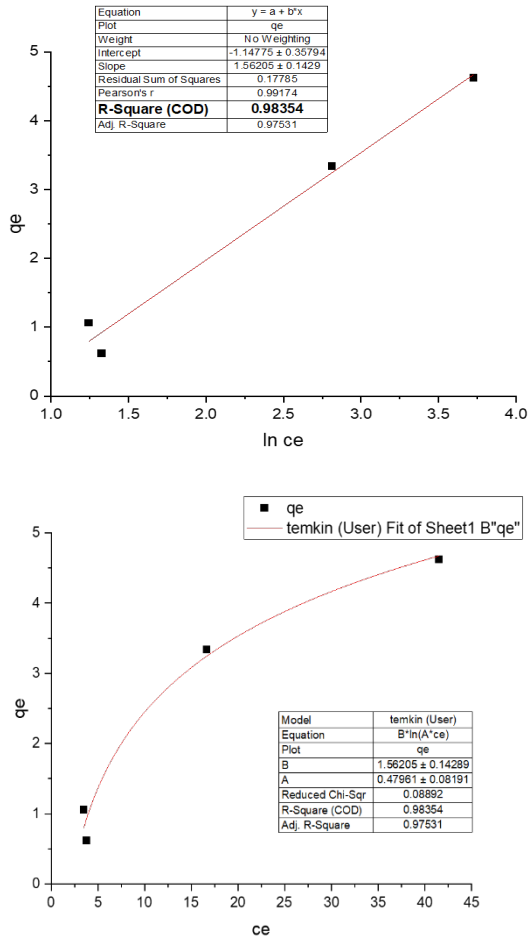

Fig. 10: Temkin isotherm model

The value of Coefficient of determination (R^2) = 0.98, Indicates the goodness of fit of the Temkin model to the experimental data. A high R^2 value close to 1 suggests that the Temkin model provides an excellent fit to the experimental adsorption data, indicating that the assumptions of the model are consistent with the observed behavior. The Temkin model fits the experimental data very well, indicating that the assumptions of the model (such as uniform adsorption energy distribution and indirect interaction between adsorbate molecules) are appropriate for describing the adsorption behaviour of fluoride onto zirconium-modified chitosan derivatives.

In summary, the adsorption process is characterized by a decrease in the heat of adsorption with increasing coverage and a uniform distribution of binding energies, as described by the Temkin isotherm model. Both nonlinear and linear models are suitable for describing this process, with the nonlinear model providing a slightly better fit as indicated by the reduced chi-square value. Because of the interactions between the adsorbent and the adsorbate, the Temkin model predicts a linear decrease in the heat of adsorption with increasing coverage. Physisorption, where the energy distribution is more uniform, is more compatible with this assumption than chemisorption, which may entail more complex and diverse binding sites. The low BT value (1.562 kJ/mol) indicates that physisorption, as instead of chemisorption, is most likely the mode of adsorption. This finding is further strengthened by the consistent model fits (both nonlinear and linear Temkin models), because the Temkin model's assumptions are in good alignment with physisorption's characteristics. As a result, the logical interpretation of the data at hand suggests that physisorption occurs during the adsorption process.

4. Conclusion:

In this study, a hybrid adsorbent was successfully developed by modifying chitosan with ethylenediamine (EDA) and zirconium using established chemical methods. The adsorbent demonstrated effective fluoride removal at initial concentrations ranging from 4 to 30 ppm. The adsorption kinetics were analyzed using pseudo-first-order (PFO), pseudo-second-order (PSO), and intraparticle diffusion (IPD) models. Nonlinear fitting of these models showed a superior correlation with the experimental data compared to linear approaches. Specifically, the adsorption process adhered to the pseudo-second-order kinetic model, the intraparticle diffusion model, and the Freundlich isotherm. The experimental data were well-described by both the Freundlich and Temkin isotherms, and moderately by the Langmuir isotherm. The kinetic and isotherm parameters were consistent with adsorption theory across the range of fluoride concentrations. The overall assessment suggests that fluoride removal is primarily driven by physisorption. This is supported by the binding energy (BT value) of 1.562 kJ/mol obtained from the IPD model, which indicates that the process is dominated by physical adsorption rather than chemical adsorption.

References

[1] S. K. Swain, S. Mishra, T. Patnaik, R. K. Patel, U. Jha, and R. K. Dey, “Fluoride removal performance of a new hybrid sorbent of Zr(IV)-ethylenediamine,” Chem. Eng. J., vol. 184, pp. 72–81, Mar. 2012, doi: 10.1016/j.cej.2011.12.091.

[2] S. Roy, S. Manna, S. Sengupta, A. Ganguli, S. Goswami, and P. Das, “Comparative assessment on defluoridation of waste water using chemical and bio-reduced graphene oxide: Batch, thermodynamic,

kinetics and optimization using response surface methodology and artificial neural network," Process Saf. Environ. Prot., vol. 111, pp. 221–231, 2017.

[3] H. Yahyavi, M. Kaykhaii, and M. Mirmoghaddam, "Recent Developments in Methods of Analysis for Fluoride Determination," Crit. Rev. Anal. Chem., vol. 46, no. 2, pp. 106–121, 2016, doi: 10.1080/10408347.2014.985814.

[4] Bhasin, C.P., Pathan, A. and Patel, R.V., 2024. An Evaluation of Carbon Nanotube-based and Activated Carbon-based Nanocomposites for Fluoride and Other Pollutant Removal from Water: A Review. Current Nanomaterials, 9(1), pp.16-40.

[5] Patel, R.V. and Bhasin, C.P., 2023. Efficient Fluoride Removal from Aqueous Solution Using Graphene/Ce Composite Supported on Activated Carbon. Current Nanomaterials, 8(4), pp.374-384.

[6] Y. Gan, X. Wang, L. Zhang, B. Wu, G. Zhang, and S. Zhang, "Coagulation removal of fluoride by zirconium tetrachloride: Performance evaluation and mechanism analysis," Chemosphere, vol. 218, pp. 860–868, 2019, doi: 10.1016/j.chemosphere.2018.11.192.

[7] J. Singh, P. Singh, and A. Singh, "Fluoride ions vs removal technologies: A study," Arab. J. Chem., vol. 9, no. 6, pp. 815–824, 2016, doi: 10.1016/j.arabjc.2014.06.005.

[8] R. Song, S. Yang, H. Xu, Z. Wang, Y. Chen, and Y. Wang, "Adsorption behavior and mechanism for the uptake of fluoride ions by reed residues," Int. J. Environ. Res. Public Health, vol. 15, no. 1, 2018, doi: 10.3390/ijerph15010101.

[9] M. M. Emamjomeh, M. Sivakumar, and A. S. Varyani, "Analysis and the understanding of fluoride removal mechanisms by an electrocoagulation/flotation (ECF) process," Desalination, vol. 275, no. 1–3, pp. 102–106, 2011, doi: 10.1016/j.desal.2011.02.032.

[10] J. Zhang, N. Chen, P. Su, M. Li, and C. Feng, "Fluoride removal from aqueous solution by Zirconium-Chitosan/Graphene Oxide Membrane," React. Funct. Polym., vol. 114, pp. 127–135, 2017, doi: 10.1016/j.reactfunctpolym.2017.03.008.

[11] Y. Zhao, "Comment on 'Zirconium-Carbon Hybrid Sorbent for Removal of Fluoride from Water: Oxalic Acid Mediated Zr(IV) Assembly and Adsorption Mechanism,'" Environ. Sci. Technol., vol. 49, no. 19, pp. 11982–11983, 2015, doi: 10.1021/acs.est.5b03792.

[12] L. H. Velazquez-Jimenez, R. H. Hurt, J. Matos, and J. R. Rangel-Mendez, "Zirconium-carbon hybrid sorbent for removal of fluoride from water: Oxalic acid mediated Zr(IV) assembly and adsorption mechanism," Environ. Sci. Technol., vol. 48, no. 2, pp. 1166–1174, 2014, doi: 10.1021/es403929b.

[13] Nayak, Tanvi, and Amanullakhan Pathan. "Environmental remediation and application of carbon-based nanomaterials in the treatment of heavy metal-contaminated water: A review." Materials Today: Proceedings (2023). doi: 10.1016/j.matpr.2023.06.227.

[14] T. L. Tan, P. A. Krusnamurthy, H. Nakajima, and S. A. Rashid, "Adsorptive, kinetics and regeneration studies of fluoride removal from water using zirconium-based metal organic frameworks," RSC Adv., vol. 10, no. 32, pp. 18740–18752, 2020, doi: 10.1039/d0ra01268h.

[15] C. H. I. Eda, "Transmittance [%] 3500 Wavenumber cm-1 1000 Instrument type and / or accessory Transmittance [%] C :\ Users \ OM \ Desktop \ LD CLG \ Uma _ Env . 0 Instrument type and / or accessory," pp. 5–6.

[16] A. Jeyaseelan and N. Viswanathan, "Facile Fabrication of Zirconium-Organic Framework-Embedded Chitosan Hybrid Spheres for Efficient Fluoride Adsorption," ACS Environ. Sci. Technol. Water, vol. 2, no. 1, pp. 52–62, 2022, doi: 10.1021/acsestwater.1c00229.

[17] M. Timur and A. Paşa, "Synthesis, Characterization, Swelling, and Metal Uptake Studies of Aryl Cross-Linked Chitosan Hydrogels," ACS Omega, vol. 3, no. 12, pp. 17416–17424, 2018, doi: 10.1021/acsomega.8b01872.

[18] Singh, K.; Lataye, D. H.; Wasewar, K. L.; Yoo, C. K. Removal of fluoride from aqueous solution: status and techniques. Desalin. Water Treat. 2013, 51, 3233−3247.

[19] Meenakshi, S.; Viswanathan, N. Identification of selective ionexchange resin for fluoride sorption. J. Colloid Interface Sci. 2007, 308, 438−450.

[20] He, J.; Chen, K.; Cai, X.; Li, Y.; Wang, C.; Zhang, K.; Jin, Z.; Meng, F.; Wang, X.; Kong, L.; Liu, J. A biocompatible and novellydefined al-hap adsorption membrane for highly effective removal of fluoride from drinking water. J. Colloid Interface Sci. 2017, 490, 97−107.

[21] Huang, H.; Liu, J.; Zhang, P.; Zhang, D.; Gao, F. Investigation on the simultaneous removal of fluoride, ammonia nitrogen and phosphate from semiconductor wastewater using chemical precipitation. Chem. Eng. J. 2017, 307, 696−706.

[22] Behbahani, M.; Moghaddam, M. R. A.; Arami, M. Technoeconomical evaluation of fluoride removal by electrocoagulation process: optimization through

response surface methodology. Desalination 2011, 271, 209−218.

[23] Pandi, K.; Viswanathan, N. Synthesis of alginate bioencapsulated nano-hydroxyapatite composite for selective fluoride sorption. Carbohydr. Polym. 2014, 112, 662−667.

[24] Pandi, K.; Viswanathan, N. A novel metal coordination enabled in carboxylated alginic acid for effective fluoride removal. Carbohydr. Polym. 2015, 118, 242−249.

[25] Maliyekkal, S. M.; Shukla, S.; Philip, L.; Nambi, I. M. Enhanced fluoride removal from drinking water by magnesia-amended activated alumina granules. Chem. Eng. J. 2008, 140, 183−192.

[26] Daifullah, A.; Yakout, S.; Elreefy, S. Adsorption of fluoride in aqueous solutions using KMnO4-modified activated carbon derived from steam pyrolysis of rice straw. J. Hazard. Mater. 2007, 147, 633−643.

[27] Nabbou, N.; Belhachemi, M.; Boumelik, M.; Merzougui, T.; Lahcene, D.; Harek, Y.; Zorpas, A. A.; Jeguirim, M. Removal of fluoride from groundwater using natural clay (kaolinite): optimization of adsorption conditions. C. R. Chim. 2019, 22, 105−112.

[28] Koilraj, P.; Kannan, S. Aqueous fluoride removal using ZnCr layered double hydroxides and their polymeric composites: batch and column studies. Chem. Eng. J. 2013, 234, 406−415.

[29] Wu, X.; Zhang, Y.; Dou, X.; Yang, M. Fluoride removal performance of a Novel Fe−Al−Ce trimetal oxide adsorbent. Chemosphere 2007, 69, 1758−1764.

[30] Jagtap, S.; Yenkie, M. K.; Labhsetwar, N.; Rayalu, S. Fluoride in drinking water and defluoridation of water. Chem. Rev. 2012, 112, 2454-2466.

[31] Patel, R.V. and Bhasin, C.P., 2022. Synthesis, Characterization and Application of Graphene/Zr Composite Supported on Activated Carbon for Efficient Removal of Fluoride from Drinking Water. Journal of Water Chemistry and Technology, 44(5), pp.344-354.

[32] Mueller, U.; Schubert, M.; Teich, F.; Puetter, H.; Schierle- Arndt, K.; Pastré, J. Metal−organic frameworks-prospective industrial applications. J. Mater. Chem. 2006, 16, 626−636.

[33] Jiang, H.-L.; Xu, Q. Porous Metal−organic frameworks as platforms for functional applications. Chem. Commun. 2011, 47, 3351-3370.

[34] Gao, Y., Li, M., Ru, Y. and Fu, J., 2021. Fluoride removal from water by using micron zirconia/zeolite molecular sieve: Characterization and echanism. Groundwater for Sustainable Development, 13, p.100567.

[35] Rahman, N. and Nasir, M., 2017. Development of Zr (IV)—Doped polypyrrole/zirconium (IV) iodate composite for efficient removal of fluoride from water environment. Journal of Water Process Engineering, 19, pp.172-184.

[36] Zhang, J., Chen, N., Su, P., Li, M. and Feng, C., 2017. Fluoride removal from aqueous solution by zirconium-chitosan/graphene oxide membrane. Reactive and Functional Polymers, 114, pp.127-135.

[37] Prathibha, C., Biswas, A., Chunduri, L.A., Reddy, S.K., Loganathan, P., Kalaruban, M. and Venkatarmaniah, K., 2020. Zr (IV) functionalized graphene oxide anchored sand as potential and economic adsorbent for fluoride removal from water. Diamond and Related Materials, 109, p.108081.

[38] Khayyun, T.S. and Mseer, A.H., 2019. Comparison of the experimental results with the Langmuir and Freundlich models for copper removal on limestone adsorbent. Applied Water Science, 9(8), p.170.